SATB2 promotes EMT-like, invasive, and endothelial tube-promoting phenotypes with the involvement of ZEB1 in 8305C anaplastic thyroid cancer cells

Lixuan Wu,[1]* Cong Wu,[1]* Xuewen Liu,[1] Qin Liu,[2] Xiaolong Wang,[1] Lei Liu,[1] Dexiang Li[1]

[1]Thyroid Surgery Department, Huizhou Central People's Hospital, Huizhou, Guangdong
[2]Hemodialysis Center, Affiliated Hospital of Huizhou Health Vocational and Technical College, Huizhou, Guangdong, China

*These authors contributed equally to the present work

ABSTRACT

Anaplastic thyroid cancer (ATC) exhibits marked dedifferentiation, rapid invasion, and limited therapeutic responsiveness. This study investigated associations between SATB2, ZEB1, EMT-like changes, invasion, short-term vemurafenib response, and endothelial tube-promoting activity in 8305C cells as an *in vitro* proof-of-concept model. SATB2 was overexpressed or silenced, followed by reciprocal ZEB1 manipulation to assess its contribution to SATB2-associated phenotypes. Expression was assessed by quantitative real-time PCR, Western blotting, and immunofluorescence. ChIP-qPCR examined SATB2 enrichment at a selected ZEB1 promoter region. Transwell assays assessed invasion, and Western blotting evaluated EMT- and angiogenesis-associated proteins. Short-term vemurafenib responses were measured using CCK-8 concentration-response assays. Supernatant VEGFA concentrations were determined by ELISA, and conditioned media were tested in HUVEC tube-formation assays. SATB2 manipulation produced concordant changes in ZEB1 mRNA and protein expression. ChIP-qPCR demonstrated significant SATB2 enrichment at the examined ZEB1 promoter region relative to IgG, indicating association without establishing direct transcriptional activation. SATB2 overexpression increased invasion, decreased E-cadherin, and increased Vimentin, VEGFA, and PDGF-BB expression; silencing produced opposite changes. SATB2 overexpression shifted the short-term vemurafenib concentration-response curve toward a higher IC_{50}, whereas silencing shifted it toward a lower IC_{50}. Reciprocal ZEB1 manipulation attenuated molecular and functional changes associated with SATB2 gain- or loss-of-function, supporting ZEB1 involvement. Conditioned medium from SATB2-overexpressing cells promoted HUVEC tube formation, which was attenuated by ZEB1 silencing. In 8305C cells, SATB2 was associated with ZEB1 expression, EMT-like remodeling, invasion, altered short-term vemurafenib response, and endothelial tube-promoting activity. Reciprocal ZEB1 manipulation supports its involvement in these phenotypes, but ChIP-qPCR does not establish direct SATB2-mediated transcriptional activation of ZEB1. Findings are limited to a single ATC cell-line model and require validation in additional experimental models.

Key words: anaplastic thyroid cancer; SATB2; ZEB1; epithelial-mesenchymal transition; vemurafenib sensitivity; angiogenesis.

Correspondence: Qin Liu, Hemodialysis Center, Affiliated Hospital of Huizhou Health Vocational and Technical College, Huizhou, Guangdong, China. E-mail: liuqinaiwlx@126.com
Lixuan Wu, Thyroid Surgery Department, Huizhou Central People's Hospital, No. 41, Eling North Road, Huicheng District, Huizhou, Guangdong 516001, China. E-mail: wulixuanailq@126.com

Contributions: Lixuan Wu, conceptualization, methodology, investigation, writing – original draft. Cong Wu, conceptualization, methodology, investigation, writing – original draft. Qin Liu, conceptualization, methodology, investigation, writing – original draft. Xuewen Liu, data curation. Xiaolong Wang, data curation. Lei Liu, formal analysis. Dexiang Li, formal analysis. All authors read and approved the final manuscript.

Conflict of interest: the authors declare no competing interests, and all authors confirm accuracy.

Data Availability Statement: the datasets used and/or analyzed during the current study are available from the corresponding author on reasonable request.

Introduction

Anaplastic thyroid cancer (ATC) is a rare but exceptionally aggressive thyroid malignancy that typically presents with rapid local expansion, early dissemination, and profound resistance to durable disease control.[1,2] Clinically, the major bottlenecks are not limited to tumor growth alone, but include extensive invasion of surrounding structures, marked intratumoral heterogeneity, rapid therapeutic escape, and the lack of stable molecular markers that can simultaneously explain malignant plasticity and treatment failure.[3,4] Although modern systemic therapy has improved the management landscape of advanced thyroid cancer, the biology of ATC remains dominated by dedifferentiation, invasion, and adaptive resistance, underscoring the urgent need to understand the necessity of ATC from a mechanism perspective.

B-Raf proto-oncogene, serine/threonine kinase (BRAF) pathway inhibition has become an important therapeutic concept in thyroid cancers carrying activating mitogen-activated protein kinase (MAPK) alterations.[5] Emerging clinical and translational studies indicate that therapeutic response is frequently incomplete, transient, or context-dependent, and that resistance is closely tied to dedifferentiation, pathway rewiring. A study conducted by Schubert indicates that resistance to BRAF inhibition can be accompanied by acquisition of secondary signaling dependencies and a more plastic state.[6] In this setting, vemurafenib remains a relevant model for interrogating how oncogenic signaling, transcriptional reprogramming, and drug responsiveness intersect in thyroid cancer cells.

Epithelial-mesenchymal transition (EMT) is a transcriptionally regulated state characterized by weakening of epithelial adhesion programs, reinforcement of mesenchymal identity, remodeling of the actin cytoskeleton, and acquisition of migratory and invasive competence.[7,8] In thyroid cancer, zinc finger E-box-binding homeobox 1 (ZEB1) has attracted particular interest because it functions as a core EMT-associated transcription factor capable of repressing epithelial identity and sustaining mesenchymal gene expression.[9] In breast cancer, Guo *et al.*[10] showed that the SIX homeobox 1 (SIX1)/ZEB1/interleukin 6 (IL6)/signal transducer and activator of transcription 3 (STAT3) signaling axis contributes to tumor progression.

Special AT-rich sequence-binding protein 2 (SATB2) is a nuclear matrix-associated chromatin regulator that influences higher-order genome organization, enhancer–promoter communication, and cell-state specification.[11] Recent mechanistic study from Gu *et al.*[12] has shown that SATB2 can shape lineage stability and chromatin architecture and thereby alter cellular plasticity.[12] Because marked dedifferentiation and transcriptional plasticity are central biological features of ATC, SATB2 was selected a priori as a hypothesis-driven candidate that might connect chromatin-associated regulation with aggressive cellular phenotypes. ZEB1 was considered a potential downstream factor because of its established role in repressing epithelial identity and promoting mesenchymal and invasive behavior in thyroid cancer. However, SATB2 was not selected on the basis of demonstrated overexpression, prognostic association, BRAF-status correlation, or transcriptomic screening in ATC, and its clinical relevance in this disease remains to be determined. Accordingly, the present study explored whether SATB2 was associated with ZEB1 expression and related malignant phenotypes in 8305C cells.

Vascular endothelial growth factor A (VEGFA) remains one of the most important pro-angiogenic effectors in solid tumors and is highly relevant to the formation of a tumor-supportive endothelial niche, while platelet-derived growth factor (PDGF)-family signaling is commonly implicated in vascular support, stromal crosstalk, and remodeling of the perivascular environment.[13] In thyroid cancer, the tumor microenvironment is not a passive backdrop but an active participant in disease lethality, with angiogenic and stromal communication contributing to the biologic distinctiveness of aggressive disease.[14] From this perspective, endothelial tube formation represents not just an isolated functional assay, but a surrogate for paracrine signaling that links tumor-cell intrinsic reprogramming to a vascular-supportive phenotype. This conceptual link is especially important in ATC, where the same plastic state that promotes invasion may also favor microenvironmental conditions that sustain progression.

In this study, using 8305C cells as an in vitro proof-of-concept model, we investigated whether SATB2 expression was associated with a ZEB1-centered program involving EMT-like remodeling, invasion, vemurafenib responsiveness, and tumor-cell-derived endothelial tube-promoting activity. The study was designed to provide preliminary mechanistic evidence rather than to establish a universally applicable pathway across molecularly heterogeneous ATC models.

Methods and Materials

Cell culture

The human ATC cell line 8305C and human umbilical vein endothelial cells were obtained from Procell (Wuhan, China). 8305C cells were maintained in RPMI-1640 medium (Gibco, Rockville, MD, USA); HUVECs were cultured in DMEM (Gibco); both RPMI-1640 and DMEM containing 10% fetal bovine serum at 37°C. Cells were passaged at approximately 70-80% confluence using routine trypsinization, and only logarithmically growing cells were used for subsequent functional and molecular assays. All tumor-cell molecular and functional experiments were conducted in 8305C cells. Accordingly, the study was designed as a cell-model-specific in vitro mechanistic analysis.

Transfection

To establish gain- and loss-of-function models, 8305C cells were transfected with a SATB2 or ZEB1 overexpression plasmid, empty vector, SATB2-targeting siRNA, ZEB1-targeting siRNA, or negative-control siRNA (si-NC). Three candidate siRNAs targeting SATB2 and three candidate siRNAs targeting ZEB1 were initially screened by qRT-PCR. The knockdown efficiencies of the individual siRNAs are shown in Figure 1A. Based on the siRNA screening results, si-SATB2#2 and si-ZEB1#2 were selected and used in all subsequent molecular and functional experiments. Transfections were performed with Lipofectamine 3000 Reagent (Invitrogen, Carlsbad, CA, USA) using Opti-MEM medium. Cells were seeded in 6-well plates one day before transfection to achieve appropriate confluence, and plasmid DNA or siRNA complexes were added in serum-free conditions for 4 h before replacement with complete medium.

The siRNA sequence is as follows: si-SATB2#1: 5'-ACAAAAGACAGGAAUCAUCAA-3'; si-SATB2#2: 5'-AUGAUAGACAUCUUGUAGCAU-3'; si-SATB2#3: 5'-UUUUCAACGUCACAACAUGAU-3'; si-ZEB1#1: 5'-AAUUUGUAACGUUAUUGCGCC-3'; si-ZEB1#2: 5'-UAAUUUGUAACGUUAUUGCGC-3'; si-ZEB1#3: 5'-AUAAUUUGUAACGUUAUUGCG-3'; si-NC: 5'-UUCUCCGAACGUGUCACGUTT-3'. Among the screened siRNAs, si-SATB2#2 (5′-AUGAUAGACAUCUUGUAGCAU-3′) and si-

OPEN ACCESS

ZEB1#2 (5′-UAAUUUGUAACGUUAUUGCGC-3′) were used in the subsequent experiments. SATB2 and ZEB1 overexpression constructs were generated using the pcDNA3.1/myc-His vector.

qRT-PCR

Total RNA was extracted from transfected 8305C cells using the Total RNA Isolation Kit V2 (Vazyme, Nanjing, China). Briefly, cells were lysed, RNA was eluted with 30 μL RNase-free ddH_2O, and RNA concentration and purity were determined using a Nano 600 spectrophotometer. For reverse transcription, 1 μg of total RNA was converted into cDNA using HiScript III All-in-one RT SuperMix Perfect for qPCR (Vazyme, Nanjing, China) with a 20 μL reaction system. The reverse-transcription program was performed at 50°C for 15 min followed by 85°C for 5 s, and the resulting cDNA was stored at -20°C until use. Quantitative PCR was then conducted using Taq Pro Universal SYBR qPCR Master Mix (Vazyme) in 20 μL reactions containing master mix, forward primer, reverse primer, RNase-free water, and 1 μL cDNA template in qPCR eight-strip tubes (Beyotime, Shanghai, China). Gene-specific primers for SATB2, ZEB1, and β-actin were synthesized by Sangon Biotech (Shanghai, China). Amplification was performed on a real-time fluorescence quantitative PCR instrument under the following cycling conditions: initial denaturation at 95°C for 30 s, followed by 40 cycles of 95°C for 10 s and 60°C for 10 s, and a final melting-curve analysis of 95°C for 15 s, 65°C for 60 s, and 95°C for 15 s. Relative mRNA expression levels were calculated using the $2^{-\Delta\Delta Ct}$ method with β-actin as the internal reference gene.

The primer sequences for qRT-PCR are as follows: SATB2 forward: 5'-CAAGGCCGTGGGAGGTTTGA-3', Reverse: 5'-ACATCTTTCCGCACCAGGAC-3'; ZEB1 forward: 5'-AGGTGTACCAGAGGATGACCT-3', Reverse: 5'-CTTGCCCTTCCTTTCCTGTGT-3'; β-actin forward: 5'-TGGCACCCAGCACAATGAA-3', Reverse: 5'-CTAAGTCATAGTCCGCCTAGAA-3'.

Chromatin immunoprecipitation–quantitative PCR

Chromatin immunoprecipitation followed by quantitative PCR was performed to assess SATB2 enrichment at the examined ZEB1 promoter region in 8305C cells. Briefly, cells were cross-linked with 1% formaldehyde for 10 min at room temperature, and the cross-linking reaction was terminated with glycine. Cells were collected and lysed, and chromatin was fragmented by sonication to obtain DNA fragments predominantly ranging from 200 to 1,000 bp. An aliquot of fragmented chromatin was retained as the input control. The remaining chromatin was incubated overnight at 4°C with an anti-SATB2 antibody obtained from Novus Biologicals, a Bio-Techne brand (catalog no. NBP1-76912), or normal rabbit IgG as the negative immunoprecipitation control. Antibody-chromatin complexes were recovered using Protein G magnetic beads, followed by washing, elution, reverse cross-linking, and DNA purification. The recovered DNA was analyzed by qPCR using primers targeting the examined human ZEB1 promoter region: forward, 5′-AAATTCAGCAGTGCCCACG-3′; reverse, 5′-TTACGACACTCCCGGCTTTAC-3′. Enrichment was calculated relative to the IgG control. The experiment was independently repeated three times.

ELISA

Culture supernatants were collected 48 h after transfection from the Vector+si-NC, OE-SATB2+si-NC, OE-SATB2+si-ZEB1, Vector+si-SATB2, and OE-ZEB1+si-SATB2 8305C groups. The supernatants were centrifuged at 1,000 × g for 5 min to remove cellular debris. VEGFA concentrations in the clarified supernatants were quantified using a Human VEGF-A ELISA Kit (Invitrogen, Thermo Fisher Scientific, Cat. No. BMS277-2) according to the manufacturer's instructions. The assay has a reported analytical sensitivity of 7.9 pg/mL and a detection range of 15.6-1,000 pg/mL. A total of 50 μL of each sample was added per well, and absorbance was measured at 450 nm using a microplate reader. VEGFA concentrations were calculated from the corresponding standard curve. Culture supernatants independently collected from separate transfection experiments constituted biological replicates, whereas replicate ELISA wells from the same supernatant were treated as technical replicates and averaged before statistical analysis. The experiment was independently repeated three times.

Western blotting

Total cellular protein was extracted with RIPA Lysis Buffer (Beyotime), and protein concentrations were determined with the Pierce BCA Protein Assay Kit (Solarbio, Beijing, China). Equal amounts of protein (20 μg) were resolved by SDS-PAGE and transferred onto 0.45 μm PVDF membranes (Beyotime). After blocking with 5% nonfat milk (Beyotime), the membranes were incubated overnight at 4°C with anti-SATB2 antibody (1:1,000, A20220), anti-ZEB1 antibody (1:1,000, A5600), anti-E-cadherin antibody (1:1,000, A19607), and anti-GAPDH antibody (1:10,000, AC001), all obtained from ABclonal (Wuhan, China); anti-Vimentin antibody (1:1,000, 5741, Cell Signaling Technology, MA, USA); and anti-VEGFA antibody (1:1,000, 81323-2-RR) and anti-PDGF-BB antibody (1:1,000, 83214-5-RR), both obtained from Proteintech (Wuhan, China). The membranes were subsequently incubated with HRP-conjugated goat anti-rabbit secondary antibody (1:5,000, SA00001-2; Proteintech, Rosemont, IL, USA). Immunoreactive signals were visualized with Pierce ECL Western Blotting Substrate (Thermo Scientific, Waltham, MA, USA) on a ChemiDoc MP Imaging System (Bio-Rad, Hercules, CA, USA). Band density was quantified with ImageJ and normalized to GAPDH. The Proteintech antibody 83214-5-RR is designated by the manufacturer as a PDGF-BB antibody and recognizes the PDGFB gene product. In the present Western blot assay using cellular protein lysates, the detected signal was interpreted as cellular PDGFB-related protein immunoreactivity rather than direct evidence of secreted, biologically active PDGF-BB homodimer.

Immunofluorescence staining

For immunofluorescence staining, transfected 8305C cells were seeded on sterile glass coverslips. The culture medium was removed, and the cells were gently washed with prewarmed PBS buffer (Beyotime). The cells were then fixed with 4% paraformaldehyde (Beyotime) at 21°C for 20 min, followed by three washes with PBS for 5 min each. For permeabilization, cells were incubated with 0.5% Triton X-100 prepared from Triton X-100 reagent (Beyotime) at 21°C for 15 min. After permeabilization, nonspecific binding was blocked with blocking buffer at 21°C for 30 min. The samples were subsequently incubated overnight at 4°C in a humidified chamber with rabbit anti-ZEB1 primary antibody (1:400). After primary antibody recovery and three PBS washes for 10 min each, the cells were incubated with ABflo® 594-conjugated secondary antibody (1:500, AS039; ABclonal) for 2 h at 21°C in the dark. F-actin was then stained with FITC Phalloidin (1:200, RM02836; ABclonal) for 30 min under light-protected conditions, followed by PBS washes. Nuclear counterstaining was performed with DAPI staining solution (1 μg/mL; Beyotime) for 10 min in the dark. Finally, the coverslips were mounted using anti-fade mounting medium (Beyotime), and fluorescence images were acquired using a fluorescence microscope (Zeiss, Oberkochen, Germany).

CCK-8 assay

The short-term metabolic viability response to vemurafenib was assessed using a CCK-8 assay. Briefly, logarithmically growing 8305C cells were seeded into 96-well plates at a density of 35,000 cells/mL and incubated at 37°C for 24 h to allow cell attachment. Vemurafenib (Y062368, Beyotime) was prepared as a stock solution and diluted with complete culture medium to final concentrations of 0.25, 0.5, 1, 2, 4, 8, 16, and 32 μM. A vehicle-control group without vemurafenib was included. Each concentration was tested in five technical replicate wells, and blank wells containing culture medium without cells were included for background correction. After 48 h of drug exposure, 10 μL of CCK-8 reagent from the CCK-8 Cell Proliferation and Cytotoxicity Assay Kit (Beyotime) was added to each well, followed by incubation for 3 h at 37°C in the dark. Absorbance at 450 nm was measured using a Multiskan FC microplate reader (357-714018, Thermo Fisher). Within each transfection condition, background-corrected absorbance values were normalized to the corresponding vehicle-treated control, which was defined as 100%. Relative metabolic viability was calculated as follows: relative metabolic viability (%) = (A_treatment − A_blank)/(A_matched vehicle control − A_blank) × 100%.

Transwell invasion assay

Cell invasion-associated activity was assessed using 24-well Transwell inserts with 8.0-μm polycarbonate membranes (Corning, Corning, NY, USA). Matrigel basement membrane matrix (Corning) was diluted 1:8 with serum-free medium, and 50 μL of the diluted Matrigel was added to each upper chamber and allowed to polymerize before cell seeding. After transfection,

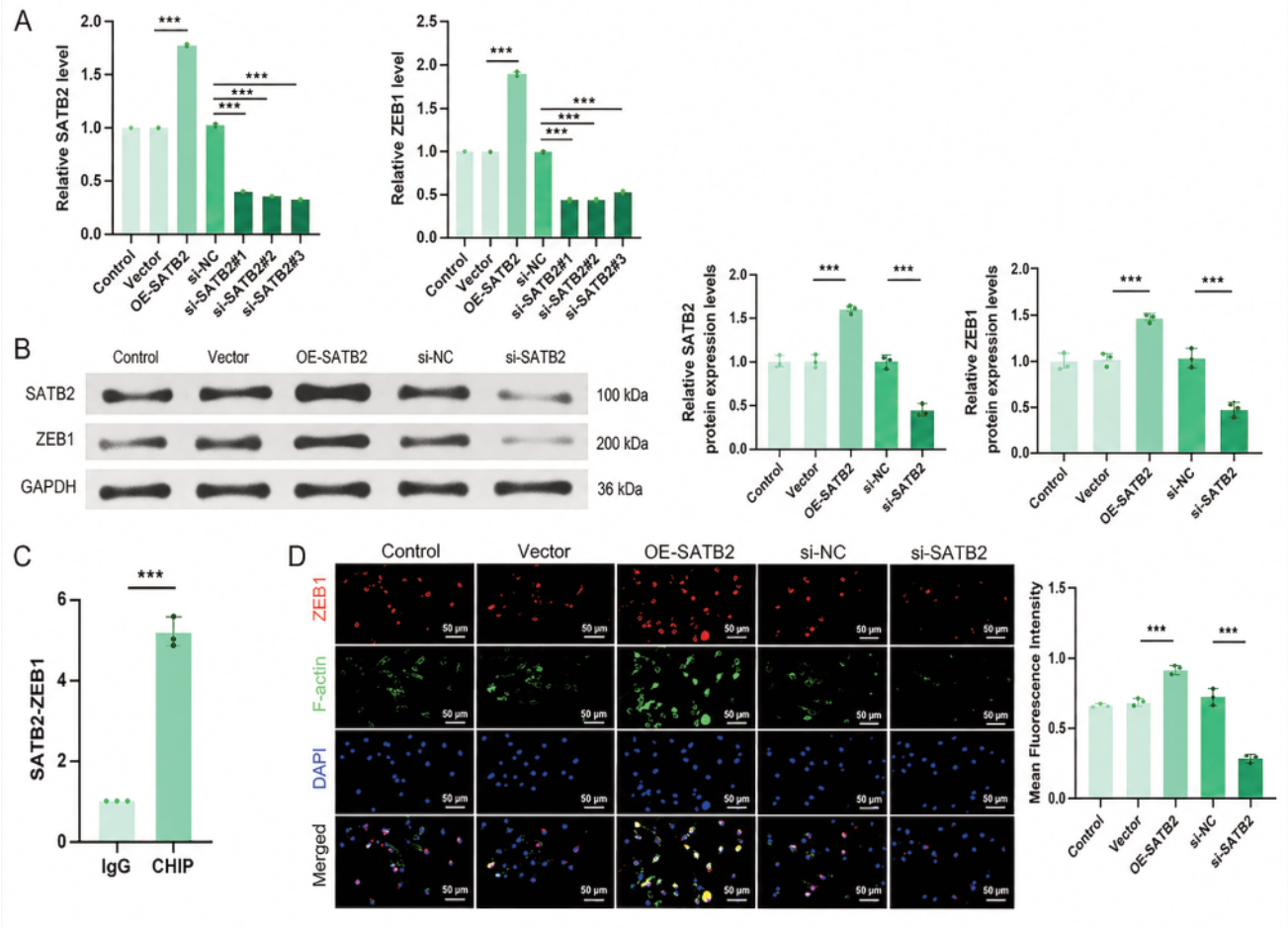


Figure 1. SATB2/ZEB1 expression and localization analyses. **A**) qRT-PCR analysis of SATB2 and ZEB1 mRNA levels in 8305C cells after SATB2 overexpression or siRNA screening; three candidate siRNAs targeting SATB2 and three candidate siRNAs targeting ZEB1 were screened, and si-SATB2#2 and si-ZEB1#2 were selected for the subsequent experiments; for qRT-PCR, RNA independently extracted from each separately cultured and transfected cell preparation constituted one biological replicate, and replicate PCR wells from the same cDNA sample were averaged before statistical analysis. **B**) Western blot analysis of SATB2, ZEB1, and GAPDH in Control, Vector, OE-SATB2, si-NC, and si-SATB2 8305C cells; each independently prepared protein lysate constituted one biological replicate, and band intensity was normalized to GAPDH. **C**) ChIP-qPCR analysis of SATB2 enrichment at the examined ZEB1 promoter region; chromatin was immunoprecipitated using an anti-SATB2 antibody or IgG as the negative control; each independently prepared chromatin sample and immunoprecipitation experiment constituted one biological replicate, and replicate qPCR wells were averaged. **D**) Immunofluorescence staining of ZEB1, F-actin, and DAPI in 8305C cells; multiple microscopic fields obtained from the same independently prepared coverslip were treated as technical subsamples and averaged to generate one biological replicate-level value; individual dots represent independent biological replicates. ***p<0.001.

OPEN ACCESS

cells from each group were harvested, prepared as single-cell suspensions, and counted. A total of 5 × 10^4 viable cells per insert were seeded into the Matrigel-coated upper chambers in serum-free medium, while complete medium containing 10% fetal bovine serum was added to the lower chambers as a chemoattractant. After 48 h of incubation, non-invaded cells remaining on the upper surface of the membrane were gently removed. Cells that had migrated through the membrane to the lower surface were fixed with methanol and stained with crystal violet. For each insert, invaded cells were counted in nine randomly selected non-overlapping microscopic fields. Three parallel inserts were analyzed for each condition within each independent experiment. Counts from the nine fields were first averaged for each insert, and the mean of the three parallel inserts was then used as one biological replicate-level value. The experiment was independently repeated three times.

Endothelial tube formation assay

Conditioned media were collected 48 h after transfection from 8305C cells in the Vector+si-NC, OE-SATB2+si-NC, OE-SATB2+si-ZEB1, Vector+si-SATB2, and OE-ZEB1+si-SATB2 groups. The culture supernatants were centrifuged at 1,000 × g for 5 min to remove cellular debris, and the serum concentration and total medium volume were adjusted to be identical among groups. For the tube-formation assay, 96-well plates were precoated with Matrigel basement membrane matrix (Corning) and incubated at 37°C to allow polymerization. HUVECs were harvested as a single-cell suspension, seeded onto the Matrigel layer, and cultured with the corresponding conditioned media collected from the indicated 8305C groups. After 12 h of incubation, endothelial network formation was photographed using an inverted microscope. Images were analyzed using ImageJ to quantify total tube length, number of branch points, and number of meshes. The experiment was independently repeated three times.

Statistical analysis

All experiments were independently repeated at least three times, and data are presented as mean ±SD. Statistical analyses were performed using GraphPad Prism 9.5. Comparisons between two independent groups were performed using two-tailed unpaired Student's *t*-tests, whereas SATB2 and IgG immunoprecipitants in the ChIP-qPCR assay were compared using a paired *t*-test. Comparisons among multiple groups were performed using one-way analysis of variance followed by Tukey's multiple-comparison test. Vemurafenib concentration–response curves were fitted using four-parameter logistic nonlinear regression, and differences between fitted curves were evaluated using the extra sum-of-squares F-test. Associations between VEGFA concentrations and tube-formation parameters were assessed using Pearson correlation analysis. Technical replicates were averaged within each independent experiment before statistical analysis. A two-sided *p*-value <0.05 was considered statistically significant.

Results

SATB2 manipulation is associated with altered ZEB1 expression and SATB2 enrichment at the ZEB1 promoter region

To investigate the relationship between SATB2 and ZEB1 in 8305C cells, SATB2 was overexpressed or silenced. qRT-PCR and western blot analyses showed that SATB2 mRNA and protein levels were markedly increased after SATB2 overexpression and decreased after SATB2 silencing (Figure 1 A,B). ZEB1 mRNA and protein expression changed in the same direction as SATB2, suggesting a positive association between SATB2 expression and ZEB1 expression. To further examine whether SATB2 was associated with the ZEB1 promoter region, ChIP-qPCR was performed using an anti-SATB2 antibody, with normal IgG serving as the negative immunoprecipitation control. The examined ZEB1 promoter fragment showed approximately fivefold greater enrichment in the SATB2 immunoprecipitated than in the IgG control (Figure 1C). This finding indicates that SATB2 is associated with the examined ZEB1 promoter region. However, promoter-region enrichment alone does not establish that SATB2 directly activates ZEB1 transcription. Immunofluorescence staining further showed stronger ZEB1 signals after SATB2 overexpression and weaker

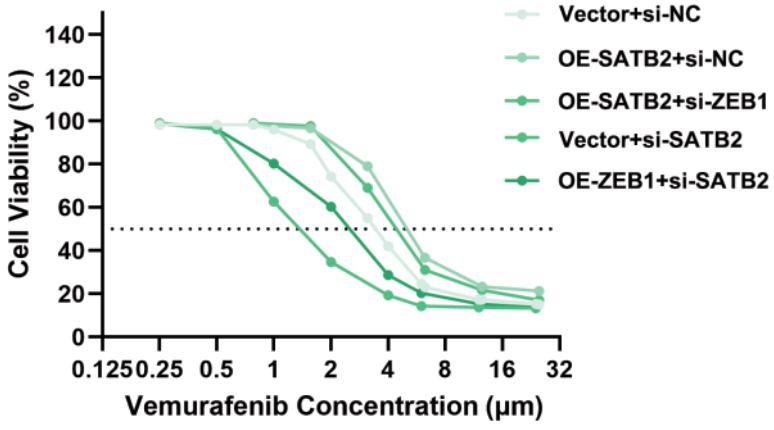


Figure 2. Short-term CCK-8-based response to vemurafenib. CCK-8-based concentration–response curves of 8305C cells treated with the indicated concentrations of vemurafenib in the Vector+si-NC, OE-SATB2+si-NC, OE-SATB2+si-ZEB1, Vector+si-SATB2, and OE-ZEB1+si-SATB2 groups. Each independent biological replicate was performed using a separately cultured and transfected batch of cells. Within each biological experiment, five wells were used as technical replicates for each vemurafenib concentration. The five technical replicate values were averaged to obtain one value per concentration for each biological replicate before curve fitting and statistical analysis.

signals after SATB2 silencing (Figure 1D). F-actin staining also revealed corresponding changes in cytoskeletal organization. Collectively, these results support a potential promoter-associated and functional relationship between SATB2 and ZEB1 expression in 8305C cells.

SATB2 alters the short-term CCK-8 response to vemurafenib with ZEB1 involvement

To examine whether SATB2 and ZEB1 manipulation was associated with the short-term response to vemurafenib, CCK-8-based concentration–response assays were performed under rescue conditions. SATB2 overexpression shifted the CCK-8 concentration–response curve rightward and increased the estimated IC_{50} from 2.951 μM in the control group to 4.218 μM, indicating an altered short-term metabolic viability response to vemurafenib. Silencing ZEB1 in SATB2-overexpressing cells attenuated this rightward shift, lowering the estimated IC_{50} to 3.63 μM. In contrast, SATB2 knockdown shifted the CCK-8 concentration–response curve leftward and reduced the estimated IC_{50} to 1.141 μM, while ZEB1 re-expression in SATB2-silenced cells attenuated this change and increased the estimated IC_{50} to 2.06 μM (Figure 2). Across the full concentration range, the rescue groups consistently showed intermediate responses between the corresponding gain- and loss-of-function groups. These results indicate that SATB2 manipulation altered the short-term CCK-8-based response to vemurafenib in 8305C cells and that the observed changes support the involvement of ZEB1.

SATB2-associated invasion is attenuated by reciprocal ZEB1 manipulation

The effect of SATB2/ZEB1 manipulation on cell invasion was evaluated using Transwell assays. SATB2 overexpression markedly increased the number of invaded cells compared with the Vector+si-NC group, whereas SATB2 knockdown significantly suppressed invasion. ZEB1 silencing in SATB2-overexpressing cells substantially reduced the increase in invaded cell numbers, whereas ZEB1 re-expression in SATB2-depleted cells attenuated the reduction in invasive ability (Figure 3). The reciprocal changes observed following ZEB1 manipulation support the involvement of ZEB1 in SATB2-associated invasive behavior in 8305C cells.

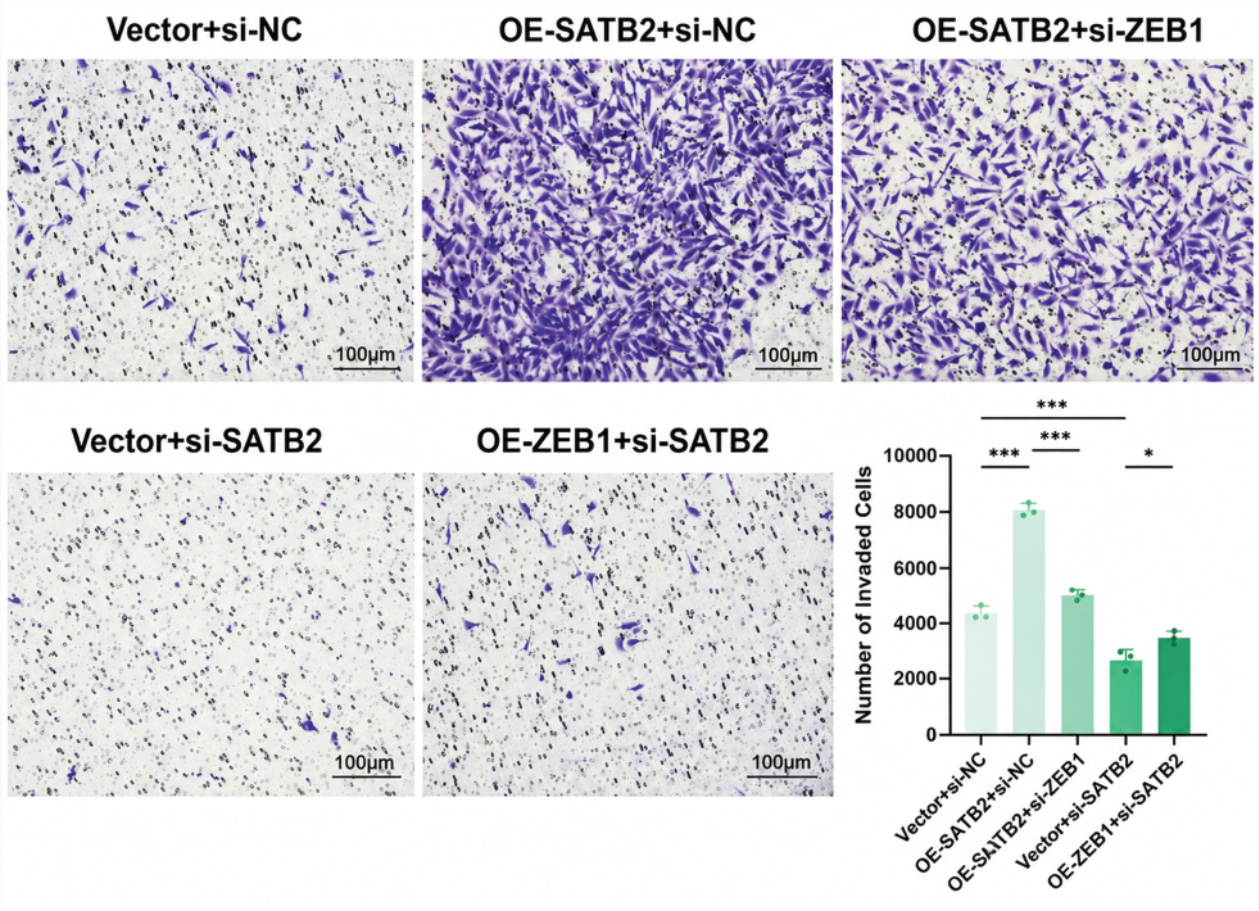


Figure 3. Transwell invasion assay. Representative images of Transwell invasion assays in Vector+si-NC, OE-SATB2+si-NC, OE-SATB2+si-ZEB1, Vector+si-SATB2, and OE-ZEB1+si-SATB2 8305C cells, together with quantification of invaded cell numbers. Within each independent experiment, three parallel Transwell inserts were prepared for each condition. Invaded cells were counted in nine randomly selected non-overlapping microscopic fields per insert. Field-level counts were first averaged for each insert, and the mean value of the three parallel inserts was used to generate one biological replicate-level value. The experiment was independently repeated three times using separately cultured and transfected cell preparations. Individual dots represent independent biological replicates. *p<0.05, ***p<0.001.

OPEN ACCESS

SATB2/ZEB1 manipulation is associated with changes in EMT-related and angiogenesis-associated proteins

To define the molecular basis of the observed phenotypic changes, EMT-related and angiogenesis-associated proteins were examined in the rescue groups. Western blot analysis showed that SATB2 overexpression reduced E-cadherin and increased Vimentin, VEGFA, and PDGF-BB levels, indicating EMT-like remodeling accompanied by changes in angiogenesis-associated protein expression. In contrast, SATB2 knockdown increased E-cadherin while decreasing Vimentin, VEGFA, and PDGF-BB expression. Importantly, these SATB2-driven molecular changes were attenuated by reciprocal manipulation of ZEB1. ZEB1 silencing in SATB2-overexpressing cells restored E-cadherin and reduced Vimentin, VEGFA, and PDGF-BB, whereas ZEB1 re-expression in SATB2-silenced cells produced the opposite trend (Figure 4). These results suggest that ZEB1 may contribute to the EMT-related molecular changes associated with SATB2 manipulation. The accompanying change in PDGF-BB should be interpreted as an angiogenesis-associated molecular alteration, because its secretion and functional contribution to endothelial tube formation were not examined.

SATB2/ZEB1 manipulation is associated with VEGFA secretion and endothelial tube-promoting activity

To further determine whether SATB2/ZEB1 manipulation is associated with the endothelial tube-promoting phenotype of anaplastic thyroid cancer cells, VEGFA levels in the corresponding culture supernatants were examined under reciprocal manipulation conditions. OE-SATB2 increased VEGFA secretion, whereas ZEB1 silencing in SATB2-overexpressing cells attenuated this increase. In contrast, si-SATB2 reduced VEGFA levels, while ectopic ZEB1 expression in SATB2-depleted cells attenuated the reduction in VEGFA secretion (Figure 5B). These findings were consistent with the western blot results for VEGFA. Functionally, conditioned medium from the OE-SATB2+si-NC group promoted a more extensive capillary-like network, with greater total tube length, more branch points, and increased mesh formation, whereas these effects were attenuated when HUVECs were cultured with conditioned medium from the OE-SATB2+si-ZEB1 group. Conversely, conditioned medium from SATB2-depleted cells impaired endothelial network formation, and this suppressive effect was attenuated by ZEB1 re-expression (Figure 5A). To further evaluate the relationship between VEGFA output and endothelial behavior, correlation analyses were performed between

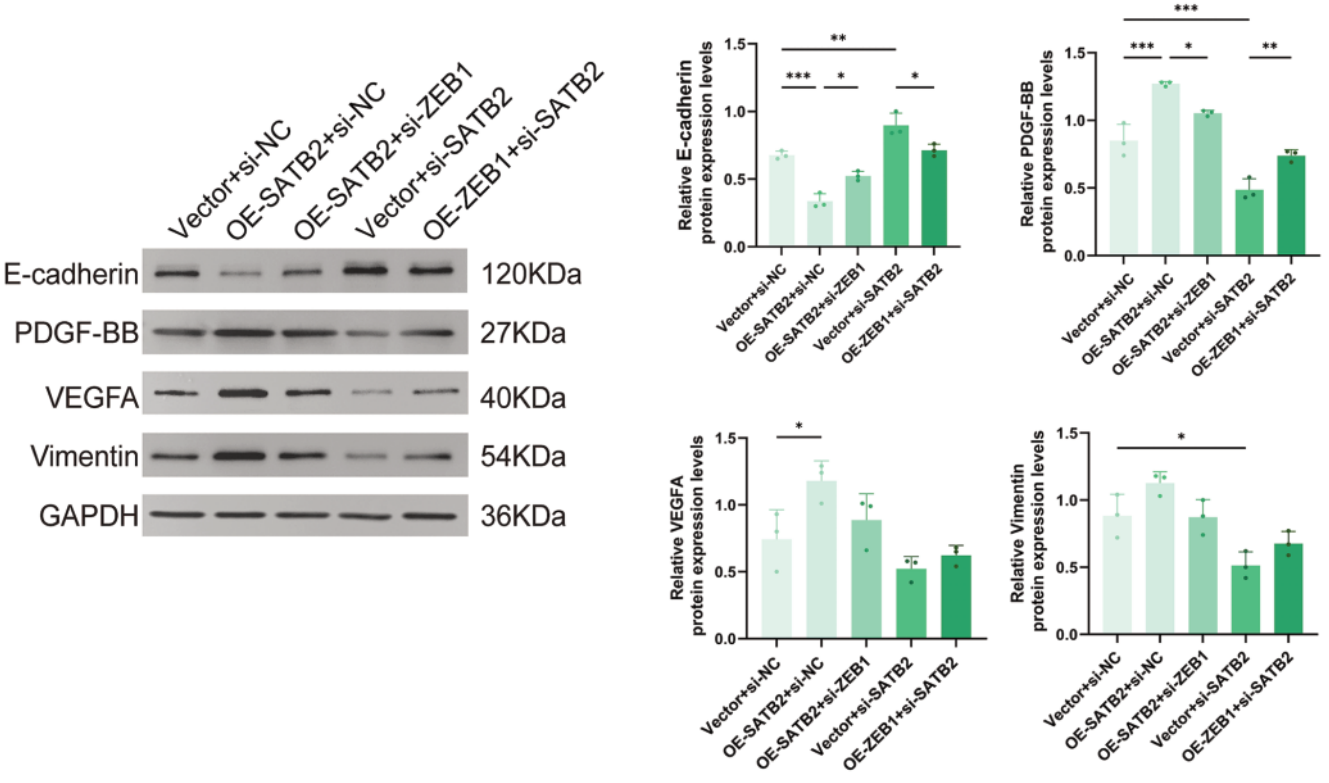


Figure 4. EMT-related and angiogenesis-associated protein analysis. Western blot analysis of E-cadherin, PDGF-BB, VEGFA, Vimentin, and GAPDH in Vector+si-NC, OE-SATB2+si-NC, OE-SATB2+si-ZEB1, Vector+si-SATB2, and OE-ZEB1+si-SATB2 8305C cells. Protein lysates independently prepared from separately cultured and transfected cells constituted the biological replicates. Band intensities were normalized to GAPDH, and each independently prepared lysate contributed one value to the statistical analysis. Individual dots represent independent biological replicates rather than repeated measurements of the same blot. *p<0.05, **p<0.01, ***p<0.001.

VEGFA concentration and the major tube-formation parameters. VEGFA levels showed positive linear associations with total tube length, branch point number, and mesh number, indicating that increased VEGFA production was closely linked to enhanced endothelial network complexity (Figure 5C). Collectively, these results indicate that VEGFA secretion levels are closely associated with the SATB2/ZEB1-related endothelial tube-promoting phenotype. However, the present data do not establish VEGFA as a causal mediator of the observed tube-formation effects.

Discussion

ATC remains the most biologically aggressive thyroid malignancy, and even though mutation-directed therapy and multimodal treatment strategies have expanded in recent years, rapid progression, invasion, and therapeutic resistance continue to limit durable control.[15] Recent single-cell analyses have shown that ATC progression is accompanied by mesenchymal tumor-cell states and extensive interactions among tumor cells, fibroblasts, endothelial cells, and immune cells, highlighting the relevance of tumor-cell plasticity and microenvironmental crosstalk in ATC.[16] Against this background, the central question motivating the present study was whether a chromatin-associated regulator could connect epithelial-mesenchymal transition, targeted-drug responsiveness, and vascular-supportive behavior in ATC. Our study addressed this question by examining the role of SATB2 in shaping ZEB1-associated malignant phenotypes and by testing whether this relationship influences EMT-associated remodeling, invasion, vemurafenib

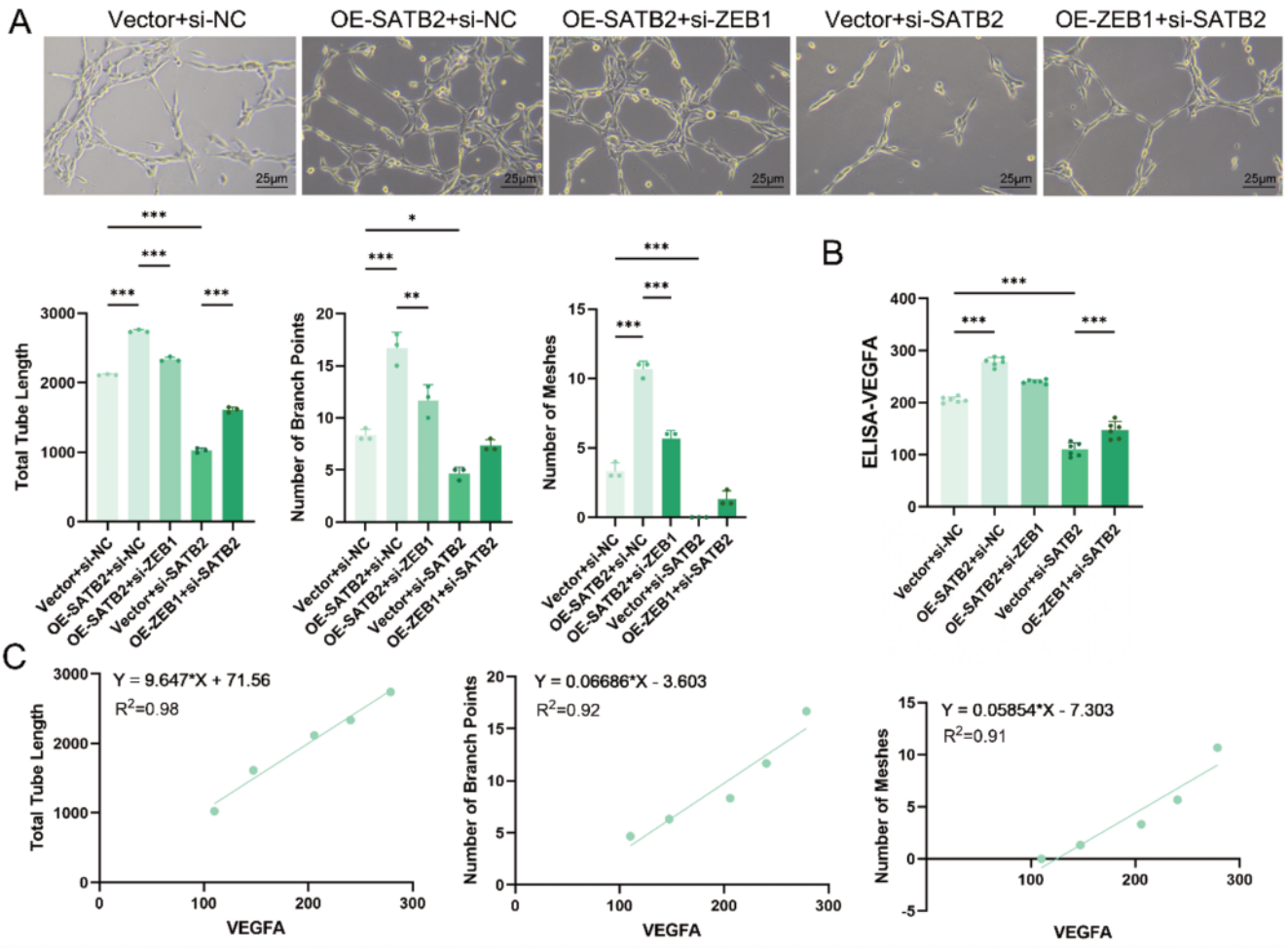


Figure 5. VEGFA secretion and endothelial tube formation analyses. **A**) Representative images of HUVEC tube formation after exposure to conditioned media collected from the indicated transfected 8305C groups; each independently performed experiment using conditioned medium collected from a separately cultured and transfected 8305C cell batch and independently seeded HUVECs constituted one biological replicate; measurements from multiple microscopic fields or wells within the same experiment were treated as technical subsamples and averaged to obtain one biological replicate-level value. **B**) ELISA analysis of VEGFA levels in culture supernatants from Vector+si-NC, OE-SATB2+si-NC, OE-SATB2+si-ZEB1, Vector+si-SATB2, and OE-ZEB1+si-SATB2 8305C cells; culture supernatants independently collected from separate transfection experiments constituted the biological replicates, whereas replicate ELISA wells from the same supernatant were treated as technical replicates and averaged before statistical analysis. **C**) Correlation analyses between VEGFA concentration and total tube length, branch point number, or mesh number; each point in the correlation plots represents the mean value of one treatment group calculated from the biological replicate-level data; technical replicate wells and microscopic fields were not entered as independent observations. Individual dots in panels A and B represent independent biological replicates. *p<0.05, **p<0.01, ***p<0.001.

OPEN ACCESS

responsiveness, and endothelial tube-promoting activity in 8305C cells. Because all tumor-cell experiments were conducted in 8305C cells, the present findings should be interpreted as proof-of-concept evidence obtained from a single *in vitro* ATC model rather than as confirmation of a universal mechanism across ATC.

SATB2 has increasingly been recognized as a context-dependent chromatin organizer capable of reshaping transcriptional programs involved in cancer progression, while epigenetic remodeling more broadly is now considered a key determinant of thyroid cancer plasticity and dedifferentiation.[12] In 8305C cells, the parallel changes in SATB2 and ZEB1, together with the rescue experiments, support a model in which SATB2 may function upstream of a ZEB1-associated mesenchymal program. This interpretation is biologically plausible because ZEB1 has already been implicated in thyroid cancer aggressiveness, EMT-associated gene regulation, and therapy-linked phenotypes in both papillary and anaplastic settings. The present results place SATB2 and ZEB1 within the same functional framework in the 8305C model, although whether this relationship is conserved across other ATC molecular backgrounds remains unknown.

The downstream phenotypes observed in our study were highly consistent with canonical EMT biology. ZEB1 is not only a marker of mesenchymal conversion, but also an active effector that represses epithelial identity, remodels the cytoskeleton, and facilitates invasive motility. In this study, SATB2 elevation was accompanied by reduced E-cadherin, increased vimentin, stronger ZEB1 immunoreactivity, more prominent F-actin organization, and greater invasive capacity, whereas SATB2 depletion produced the opposite pattern. These findings support the view that SATB2 reinforces a ZEB1-centered mesenchymal state. The rescue experiments were particularly informative because ZEB1 silencing attenuated the pro-invasive and EMT-like effects of SATB2 overexpression, whereas re-expression of ZEB1 attenuated the corresponding changes after SATB2 knockdown. In the broader thyroid cancer literature, ZEB1-linked transcriptional programs have similarly been connected to EMT, metastatic competence, and aggressive disease behavior, which strengthens the biological plausibility of the mechanism proposed here.[17]

Although BRAF-directed strategies have become important for molecularly selected thyroid cancers, incomplete response and adaptive resistance remain major clinical obstacles. Recent studies have shown that vemurafenib-exposed thyroid cancer cells can engage stemness-associated and compensatory signaling programs, while ZEB1-associated networks in ATC can also shape treatment response in other settings.[18,19] Within this context, our observation that SATB2 manipulation shifted the short-term CCK-8 concentration-response profile for vemurafenib, and that reciprocal ZEB1 manipulation attenuated this shift, suggests that SATB2 and ZEB1 are associated with changes in the short-term metabolic viability response to vemurafenib in 8305C cells. Because CCK-8 reflects cellular metabolic activity, these findings cannot distinguish altered drug responsiveness from differences in baseline proliferation, survival, or metabolism caused by SATB2 or ZEB1 manipulation. Accordingly, the present findings support the involvement of ZEB1 but do not quantify the extent to which ZEB1 accounts for the SATB2-associated vemurafenib response.

Recent single-cell analysis of ATC has identified distinct stromal and endothelial compartments and increased VEGF- and PDGF-related cell-cell communication involving endothelial cells, supporting the relevance of vascular and stromal crosstalk in the ATC microenvironment.[20] In our study, SATB2 overexpression increased VEGFA and PDGF-BB protein expression and was accompanied by enhanced HUVEC tube formation, whereas SATB2 depletion produced the opposite pattern. Reciprocal ZEB1 manipulation attenuated these changes. These results suggest that SATB2/ZEB1 manipulation is associated not only with EMT-related changes in tumor cells but also with tumor-cell-derived signals that influence HUVEC tube-like structure formation in vitro. These findings are consistent with previous ATC-specific evidence linking ZEB1- and VEGFA-related changes with EMT, invasion, and endothelial tube formation.[21] Nevertheless, because VEGFA was not specifically blocked or supplemented in the conditioned-medium experiments, the present findings demonstrate an association between VEGFA secretion and endothelial tube formation but do not establish VEGFA as the causal mediator of this phenotype. Unlike VEGFA, PDGF-BB was not measured in the culture supernatants and was not examined in relation to the tube-formation parameters. Therefore, the present data only show that PDGF-BB protein expression changes in parallel with SATB2/ZEB1 manipulation and do not establish PDGF-BB as a secreted or functionally validated mediator of the endothelial phenotype.

This study has limitations. First, all tumor-cell molecular and functional experiments were performed in the 8305C cell line. ATC is molecularly heterogeneous, and the direction or magnitude of SATB2/ZEB1-associated phenotypes may differ among cell models with distinct BRAF, RAS, TP53, TERT, and other genomic backgrounds. Therefore, the present results should be regarded as cell-model-specific proof-of-concept evidence. Validation in additional BRAF-mutant and BRAF-wild-type ATC models will be necessary before the findings can be generalized to ATC as a disease entity. Second, although SATB2 enrichment was detected at the examined ZEB1 promoter region and ZEB1 expression changed in parallel with SATB2 manipulation, the present findings do not establish direct transcriptional activation. ChIP-qPCR demonstrates protein enrichment or occupancy at a selected genomic region, whereas promoter-reporter and binding-site mutation analyses would be required to determine whether SATB2 directly activates ZEB1 transcription. Therefore, cofactor-dependent or indirect regulation cannot be excluded. Third, vemurafenib response was evaluated using a 48-h CCK-8 assay. Because CCK-8 measures metabolic activity rather than proliferation or cell death directly, differences in baseline growth, survival, or metabolism after SATB2 and ZEB1 manipulation may have contributed to the observed concentration-response profiles. Although the data were normalized to the matched vehicle control within each transfection group, this approach cannot fully exclude such confounding. Therefore, the CCK-8-derived IC_{50} values should be interpreted as indicators of short-term metabolic viability response, and confirmation using clonogenic and apoptosis-based assays is warranted. Fourth, the HUVEC tube-formation assay is an in vitro surrogate assay that reflects the ability of endothelial cells to form tube-like structures on Matrigel. It does not reproduce the complete process of tumor angiogenesis, which also involves endothelial migration, proliferation, vascular maturation, and interactions with other components of the tumor microenvironment. Therefore, the present findings should be interpreted as evidence of endothelial tube-promoting activity rather than definitive evidence of tumor angiogenesis. Finally, correlation with human ATC tissues and clinicopathologic annotation will be required before SATB2/ZEB1 can be advanced as a biomarker-guided therapeutic target.

This study identifies an association between SATB2/ZEB1-related regulation and EMT-like remodeling, invasion, reduced short-term CCK-8-based responsiveness to vemurafenib, and endothelial tube-promoting activity in 8305C cells. These findings provide preliminary, cell-model-specific evidence supporting further investigation of the relationship between SATB2 and ZEB1 in ATC.

References

1. Bible KC, Kebebew E, Brierley J, Brito JP, Cabanillas ME, Clark TJ, Jr. et al. 2021 American Thyroid Association guidelines for management of patients with anaplastic thyroid cancer. Thyroid 2021;31:337-86.
2. Rao SN, Smallridge RC. Anaplastic thyroid cancer: An update. Best Pract Res Clin Endocrinol Metab 2023;37:101678.
3. Alobuia W, Gillis A, Kebebew E. Contemporary management of anaplastic thyroid cancer. Curr Treat Options Oncol 2020;21:78.
4. Dey T, Yadav BS. Anaplastic thyroid cancer: Unveiling advances in diagnosis and management. World J Clin Oncol 2024;15:786-9.
5. Scheffel RS, Dora JM, Maia AL. BRAF mutations in thyroid cancer. Curr Opin Oncol 2022;34:9-18.
6. Schubert L, Mariko ML, Clerc J, Huillard O, Groussin L. MAPK pathway inhibitors in thyroid cancer: preclinical and clinical data. Cancers (Basel) 2023;15.
7. Basu A, Paul MK, Weiss S. The actin cytoskeleton: morphological changes in pre- and fully developed lung cancer. Biophys Rev (Melville) 2022;3:041304.
8. Zhang YE, Stuelten CH. Alternative splicing in EMT and TGF-beta signaling during cancer progression. Semin Cancer Biol 2024;101:1-11.
9. Park JH, Myung JK, Lee SJ, Kim H, Kim S, Lee SB, et al. ABCA1-mediated EMT Promotes papillary thyroid cancer malignancy through the ERK/Fra-1/ZEB1 pathway. Cells 2023;12.
10. Guo L, Rao Y, Song Y, Hu J, Luo Z, Sun S, et al. SIX1 transmits signals for breast cancer progression via the ZEB1/IL6/STAT3 signaling axis. Oncogene 2025;44:3493-511.
11. Kowalczyk AE, Sliwinska-Jewsiewicka A, Krazinski BE, Piotrowska A, Grzegrzolka J, Godlewski J, et al. Reduced expression of SATB2 in colorectal cancer and its association with demographic and clinicopathological parameters. Int J Mol Sci 2025;26.
12. Gu W, Wang H, Huang X, Kraiczy J, Singh PNP, Ng C, et al. SATB2 preserves colon stem cell identity and mediates ileum-colon conversion via enhancer remodeling. Cell Stem Cell 2022;29:101-15 e10.
13. Chen L, Xie X, Wang T, Xu L, Zhai Z, Wu H, et al. ARL13B promotes angiogenesis and glioma growth by activating VEGFA-VEGFR2 signaling. Neuro Oncol 2023;25:871-85.
14. Chen Q, Yu WY, Zhang HH, Zhang SZ, Fang J, Wu F, et al. PBX3 promotes tumor growth and angiogenesis via activation of AT1R/VEGFR2 pathway in papillary thyroid carcinoma. Biomed Res Int 2020;2020:8954513.
15. Shaha AR. Anaplastic thyroid cancer: shifting paradigms-A ray of hope. Thyroid 2023;33:402-3.
16. Lu L, Wang JR, Henderson YC, Bai S, Yang J, Hu M, et al. Anaplastic transformation in thyroid cancer revealed by single-cell transcriptomics. J Clin Invest 2023;133:e169653.
17. Liu W, Lin R, Zhu C, Chen Y, Gao Q, Zhong J. CCT2 regulates ZEB1-induced EMT gene transcription to promote the metastasis and tumorigenesis of papillary thyroid carcinoma. Discov Med 2024;36:1819-30.
18. Lu Y, Zhao Y, Liu P, Xu X. Vemurafenib activates the sonic hedgehog pathway and promotes thyroid cancer stem cell self-renewal. Endocr Relat Cancer 2023;30.
19. Zhao Y, Lu Y, Li W, Liu P, Xu X. Acquired resistance to vemurafenib restrains thyroid cancer stem cell self-renewal by suppressing STAT3 activation. Cell Signal 2025;133:111845.
20. Han PZ, Ye WD, Yu PC, Tan LC, Shi X, Chen XF, et al. A distinct tumor microenvironment makes anaplastic thyroid cancer more lethal but immunotherapy sensitive than papillary thyroid cancer. JCI Insight 2024;9:e173712.
21. Vosgha H, Ariana A, Smith RA, Lam AKY. miR-205 targets angiogenesis and EMT concurrently in anaplastic thyroid carcinoma. Endocr Relat Cancer 2018;25:323-37.

Received: 21 July 2026. Accepted: 18 September 2026.

This work is licensed under a Creative Commons Attribution-NonCommercial 4.0 International License (CC BY-NC 4.0).
©Copyright: the Author(s), 2026
Licensee PAGEPress, Italy
European Journal of Histochemistry 2026; 70:4738
doi:10.4081/ejh.2026.4738

Publisher's note: all claims expressed in this article are solely those of the authors and do not necessarily represent those of their affiliated organizations, or those of the publisher, the editors and the reviewers. Any product that may be evaluated in this article or claim that may be made by its manufacturer is not guaranteed or endorsed by the publisher.

OPEN ACCESS